Catalysis Science & Technology

ROYAL SOCIETY OF CHEMISTRY

PAPER

View Article Online
View Journal | View Issue

Cite this: *Catal. Sci. Technol.*, 2024, **14**, 646

Bulky olefin epoxidation under mild conditions over Mo-based oxide catalysts†

Diana M. Gomes,[a] Xingyu Yao,[b] Patrícia Neves,*[a] Nicola Pinna,[b] Patrícia A. Russo[b] and Anabela A. Valente *[a]

Received 17th September 2023,
Accepted 1st January 2024

DOI: 10.1039/d3cy01299a

rsc.li/catalysis

Molybdenum-based epoxidation catalysts are among the most investigated since the homogeneous Mo-based catalytic process claimed by Halcon International Inc. for liquid phase olefin epoxidation (EPO). While homogeneous Mo-based catalytic technologies reached industrial implementation for olefin EPO, the same does not apply for heterogeneous Mo-based ones, which have not reached industrial implementation (*e.g.*, to meet catalyst productivity and stability requirements). In this work, EPO nanocatalysts consisting of oxides possessing molybdenum and M = Ta, Nb or W were prepared *via* a simple, versatile methodology. The influence of the material synthesis conditions on the material properties was investigated to meet superior catalytic performances. Promising Mo-based solid catalysts were obtained which promoted the EPO of relatively bulky olefins such as fatty acid methyl esters (methyl oleate, methyl linoleate), using *tert*-butyl hydroperoxide as oxidant under mild conditions; *e.g.*, the materials Mo(75D)M-0.3 with M = Nb, W (75 at% Mo relative to M, and MoO_2Cl_2 as precursor), obtained in a fast synthesis of 0.3 h, led to 92–96% epoxide selectivity at 84–95% methyl oleate conversion, at 70 °C. To the best of our knowledge, these are the first Mo,M oxides reported for these reactions.

Introduction

The chemical valorisation of olefins *via* epoxidation (EPO) routes is of great industrial relevance because epoxides are important intermediates to many end use industries.[1,2] In the search for more efficient epoxides production routes, EPO technologies have evolved from hazardous stoichiometric processes to greener catalytic processes, and the latter are shifting from homogeneous to heterogeneous catalysis.[3,4] For example, the industrial heterogeneous catalytic EPO process known as hydrogen peroxide–propylene oxide technology (HPPO) uses a titanium silicalite-1 (TS-1) type catalyst, which is a crystalline microporous material possessing an MFI topology consisting of (medium pore) 10-memberred ring channels with *ca.* 5.5 Å width.[1,5–7] While this catalyst is suitable for small reactant molecules, such as light olefins and H_2O_2 as oxidant, it may be impractical for reactions involving relatively bulky olefins and/or oxidant molecules (*e.g.*, organic hydroperoxides) due to its reduced pore sizes.[8] This drawback gains considerable relevance in times where the chemical industry faces challenges to use renewable sources of organic carbon, such as relatively bulky vegetable biomass components[9,10] which includes fatty acid esters with varying degrees of unsaturation.[11]

Relatively bulky fatty acid methyl esters (FAMEs) are important industrial chemicals with a growing market (Scheme 1).[9,12,13] The EPO of FAMEs gives epoxy fatty acid methyl esters (EFAMEs) with environmentally friendly characteristics such as biodegradability and nontoxicity.[14] EFAMEs have a growing global market with a broad applications

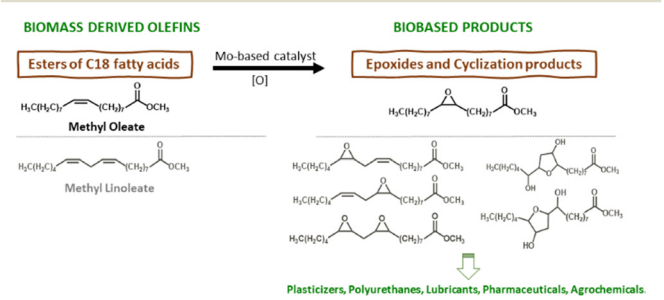

Scheme 1 Chemical valorisation of fatty acid methyl esters (FAMEs) obtainable from food/agricultural/industrial waste or surpluses, *via* catalytic epoxidation (EPO) routes to useful epoxides.

[a] *Department of Chemistry, CICECO-Aveiro Institute of Materials, University of Aveiro, Campus Universitário de Santiago, 3810-193 Aveiro, Portugal. E-mail: pneves@ua.pt, atav@ua.pt*
[b] *Department of Chemistry, IRIS Adlershof & The Center for the Science of Materials Berlin, Humboldt-Universität zu Berlin, Brook-Taylor-Str. 2, 12489 Berlin, Germany*

† Electronic supplementary information (ESI) available: Characterisation of Mo, M oxides (composition, textural properties, DR UV-vis), M_xO_y (PXRD, TEM, SEM, ATR FT-IR) and used catalysts (PXRD, TEM, SEM, STEM, composition, DR UV-vis, ATR FT-IR). Catalytic results (influence of material properties on the initial activities, kinetic profiles for MeLin). See DOI: https://doi.org/10.1039/d3cy01299a

profile, *e.g.*, solvents, plasticizers, lubricants, biofuels.[5,12,15–24] However, heterogeneous catalytic EPO of FAMEs presents challenges, such as the development of highly active, selective and stable catalysts, using catalyst synthesis methodologies which are timesaving and versatile (*e.g.*, possibility of introducing different metals to meet superior performances).[14] In the choice of the types of catalytic materials, fully inorganic metal oxides may be preferable to materials possessing organic components, in what concerns thermal and chemical stabilities. Moreover, some monometallic or mixed metal oxides may be prepared *via* synthesis strategies which only require the metal precursors and an appropriate solvent (advantageous in relation to ordered mesoporous metal/metalloid oxides synthesized using organic templates which need to be subsequently destroyed), with the possibility of offering some control over the crystallinity, size and morphology of the materials.[25,26]

Molybdenum-based EPO catalysts are promising and among the most investigated since the homogeneous Mo-based catalytic EPO process claimed by Halcon International Inc. (USA) in the 1960s.[27–30] While homogeneous Mo-based catalytic technologies reached industrial implementation for olefin EPO, the same does not apply for heterogeneous Mo-based ones, which continue of great interest, albeit challenging, *e.g.* to meet the catalyst productivity and stability requirements.[31–33]

Besides molybdenum, different metal oxides were reported for olefin EPO, such as niobium, tantalum and tungsten oxides.[34] To the best of our knowledge, mixtures of Mo oxide with oxides of Nb, Ta or W were not investigated for liquid phase EPO. According to the literature, precursors of group 5 metals (*e.g.*, niobic acid, Ta_2O_5) may react with several other precursors, such as molybdenum of group 6 (*e.g.*, $(NH_4)_6Mo_7O_{24}{\cdot}4H_2O$, MoO_3), to form multimetallic oxides,[35,36] which may result in improved catalytic performance for different oxidation systems.[37] For example, it was reported that the presence of niobium in mixed oxide materials containing molybdenum (which is redox flexible) may enhance the material's stability towards oxidation/reduction. Moreover, niobium and tantalum may confer high mechanical and corrosion resistance to materials.[38]

In this work, EPO catalysts consisting of Mo and M = Ta, Nb or W oxides were prepared *via* a simple and versatile non-aqueous sol–gel synthesis, using acetophenone as solvent. According to ECHA, acetophenone presents biodegradability and low aquatic toxicity properties towards the environment.[39] These catalytic materials promoted the EPO of relatively bulky olefins. The influence of the type and concentration of the molybdenum precursor and synthesis time on the material properties and catalytic performances were firstly investigated, based on the model reaction of *cis*-cyclooctene (Cy) using *tert*-butylhydroperoxide as oxidant, at 70 °C. The catalytic stability was studied by performing consecutive catalytic runs and characterising the recovered solids. The best-performing catalysts were explored for the EPO of the biobased FAMEs methyl oleate and methyl linoleate. The Mo,M oxides were more effective than the monometallic oxides M_xO_y, and relatively stable Mo,Nb- and Mo,W oxides promoted the conversion of the FAMEs; *e.g.*, Mo(75D)M-0.3 with M = Nb, W (material synthesis time of 0.3 h, using 75 at% Mo relative to M, and MoO_2Cl_2 as precursor), led to 92–93% epoxide selectivity at 90–95% methyl oleate conversion.

Experimental

Materials

The following reagents and chemicals were purchased from Sigma-Aldrich, unless otherwise stated, and used as received. Synthesis: acetophenone (99.9%), molybdenum(VI) dichloride dioxide, tungsten(VI) chloride (≥99.9%), tantalum(V) chloride (99.8%, Alfa Aesar), and niobium(V) chloride (99.95%, ABCR). Catalysis: *cis*-cyclooctene (95%, Alfa Aesar), methyl oleate (99%), methyl linoleate (95%, Alfa Aesar), *tert*-butylhydroperoxide (5.5 M in decane, containing *ca.* 4% water), anhydrous α,α,α-trifluorotoluene (≥99%), acetone (99.5%, Honeywell, Riedel de Häen), 1,2-dichloroethane (≥99%), methyl decanoate (99%), undecane (>99%), and the crystalline oxides MoO_2 (99%), MoO_3 (99.5%, VWR), WO_3 (99%, Fluka), Nb_2O_5 (99.99%, Fluka) and Ta_2O_5 (99.99%, PI-KEM).

Synthesis of the catalysts

In a typical synthesis, 20 mL of acetophenone and a total of 0.5 mmol of the metal precursors ($TaCl_5$, $NbCl_5$, WCl_6, and/or $MoCl_5$ or MoO_2Cl_2) in the desired molar proportions, were added to a microwave glass vial in a glovebox. The vial was heated in an Anton Paar Monowave 300 microwave reactor, at 220 °C for 20 min. The solid product was separated by centrifugation, washed four times with 20 mL of acetone and ethanol, and dried at 65 °C for 12 h. The 24 h reactions (for selected materials) were carried out in a similar fashion, albeit using a Teflon-cup-lined stainless steel autoclave.[25,40] The Mo,M oxide materials are denoted Mo(*x*D)M-*t* or Mo(*x*P)M-*t* where *x* is the normalized at% of Mo relative to M of the synthesis mixture (*i.e.*, *x* = 25, 50 and 75 for a ratio Mo : M of 25 : 75, 50 : 50 and 75 : 25, respectively), *t* is the material synthesis time, and D corresponds to the use of MoO_2Cl_2 as precursor and P corresponds to the use of $MoCl_5$ as precursor.

Characterization of the catalysts

Powder X-ray diffraction (PXRD) data were collected on an Empyrean PANalytical diffractometer (Cu-K_α X-radiation, λ = 1.54060 Å) equipped with a spinning flat sample holder and a PIXcel 1D detector set at 240 mm from the sample, in a Bragg–Brentano *para*-focusing optics configuration (45 kV, 40 mA) at ambient temperature. Samples were prepared in a spinning flat plate sample holder and step-scanned from 3 to 70° (2θ) in 0.026° 2θ steps with a counting time of 90 s per step.

Scanning electron microscopy (SEM) images and EDS analyses were obtained on a Hitachi SU-70 SEM microscope equipped with a Bruker Quantax 400 detector operating at 15 kV. Samples were prepared by deposition on aluminum sample holders followed by carbon coating using an Emitech K 950 carbon evaporator. Transmission electron microscopy (TEM), high resolution TEM (HRTEM), high angle annular dark field scanning transmission electron microscopy (HAADF-STEM), and elemental mapping analyses were carried out on a FEI Talos F200S scanning/transmission electron microscope (S/TEM) operated at 200 kV, and a Hitachi HD2700 microscope equipped with a Bruker Quantax SVE 6 EDS detector operating at 80–200 kV.

The textural properties were determined from the N_2 sorption isotherms at −196 °C, which were measured using a Quantachrome instrument (automated gas sorption data using Autosorb IQ2, Quantachrome Instruments). The sample was pre-treated at 170 °C for 3 h, under vacuum ($<4 \times 10^{-3}$ bar). The specific surface area was calculated using the Brunauer, Emmett, Teller equation (S_{BET}).

ICP-OES analyses (for Mo, W, Nb and Ta) were performed at the Central Analysis Laboratory (University of Aveiro); the measurements were carried out on a Horiba Jobin Yvon Activa M spectrometer (detection limit of *ca.* 20 μg dm^{-3}; experimental range of error of *ca.* 5%). Prior to analysis, 10 mg of solid sample was digested using 0.5 mL HF and 0.5 mL HNO_3, and microwave heating at 180 °C.

Attenuated total reflectance (ATR) FT-IR spectra were measured on a Bruker Tensor 27 spectrophotometer equipped with a Specac® Golden Gate Mk II ATR accessory having a diamond top plate and KRS-5 focusing lenses (resolution 4 cm^{-1}, 256 scans). Diffuse reflectance (DR) UV-vis spectra were recorded using a JASCO V-780 spectrophotometer equipped with a JASCO ISV-469 integrating sphere coated with barium sulfate, with light detection by a built-in photomultiplier tube attached to the base of the sphere. The spectra were collected in reflectance mode with a wavelength scan speed of 200 nm min^{-1}, step size of 0.5 nm, and a slit width of 2.0 nm.

Catalytic tests

The catalytic reactions were carried out in borosilicate reactors equipped with a Teflon valve for sampling and a magnetic stirrer. Initially, the catalyst (5.6 g_{cat} per mole of olefin), substrate and solvent (α,α,α-trifluorotoluene (TFT)) were added to the reactor, which was then immersed in a temperature-controlled oil bath at 70 °C, under stirring (1000 rpm, optimized to avoid mass transfer limitations). After 10 min, the preheated oxidant, namely *tert*-butylhydroperoxide (TBHP), was added to the reactor, and this moment was taken as the initial instant of the catalytic reaction. For the model reaction of *cis*-cyclooctene (Cy), the initial reaction conditions were *ca.* 1 M Cy and mole ratio TBHP : Cy = 1.5. For the biobased FAMEs, namely methyl oleate (MeOle) and methyl linoleate (MeLin), the initial reaction conditions were *ca.* 0.5 M FAME, and TBHP : FAME = 1.5 for MeOle or 2.5 for MeLin.

The evolution of the reactions was monitored by analyzing freshly prepared samples by gas chromatography (GC), using a Varian 450 GC instrument equipped with a BR-5 capillary column (30 m × 0.25 mm × 0.25 μm) and an FID detector with H_2 as carrier gas. The quantifications of the reactants and products were based on calibrations (the internal standard was undecane for Cy, and methyl decanoate for bioolefins). The initial activity (mmol g_{cat}^{-1} h^{-1}) was calculated based on olefin conversion at 1 h reaction. The reaction products were identified by GC-MS (GC MS QP2010 Ultra Shimadzu), using He as the carrier gas; the product identifications were based on commercial mass spectrometry databases (Wiley229, NIST14, NIST Chemistry WebBook, MAINLIB) and mass spectra similarities. The products' mass spectra were reported previously.[41,42]

The catalyst stability was evaluated by reusing the recovered solids in consecutive batch runs, keeping constant the initial mass ratio of catalyst : Cy : TBHP between runs. After each run, the solids were separated from the reaction mixture by centrifugation (3500 rpm), thoroughly washed with acetone, dried overnight under air atmosphere, and finally vacuum-dried (*ca.* 0.1 bar) at 60 °C for 1 h.

Results and discussion

Characterization of the materials

Chemical composition of the metal oxides. The monometallic oxides M_xO_y (M = Mo, Ta, Nb, W) and the Mo, M oxides Mo(*x*D)M-*t* and Mo(*x*P)M-*t* were prepared *via* simple, one-pot solvothermal syntheses from the respective metal (M, Mo) precursors and acetophenone (*t* = synthesis time; *x*D and *x*P = normalized (*x*) at% of Mo relative to M, using the precursor D = MoO_2Cl_2 or P = $MoCl_5$). Given the relevance of molybdenum sites for catalytic EPO (described in the Introduction section), the influence of the type and amount of the Mo precursor, as well as of the synthesis time on the materials properties were investigated.

The mole ratios of the materials (Mo/M), as well as those of the respective synthesis (Syn) mixtures ($(Mo/M)_{Syn}$ = 0.3, 1 or 3 for *x* = 25, 50 and 75, respectively) are indicated in Fig. S1.† In general, Mo(*x*D)M-0.3 and Mo(*x*P)M-0.3 possessed lower Mo/M than the respective $(Mo/M)_{Syn}$, indicating that not all metal content of the synthesis mixture was incorporated in these materials. Increasing the synthesis time from 0.3 h to 24 h led to higher Mo/M; *e.g.*, the Mo/M ratios of Mo(50D)M-0.3 *versus* Mo(50D)M-24 (both synthesized using $(Mo/M)_{Syn}$ = 1) were in the ranges 0.10–0.23 and 0.54–0.86, respectively.

On the other hand, the influence of the type of Mo precursor (D or P) was studied for the Mo,M oxides with M = W, Nb and *x* = 25, 50, or with M = Ta and *x* = 50. The D precursor led to higher Mo/M than the P one, *e.g.*, Mo(50D)W-0.3 possessed approximately double the Mo/M ratio of Mo(50P)W-0.3 (0.23 and 0.12, respectively). Hence, MoO_2Cl_2 seemed more favorable for introducing molybdenum in the materials.

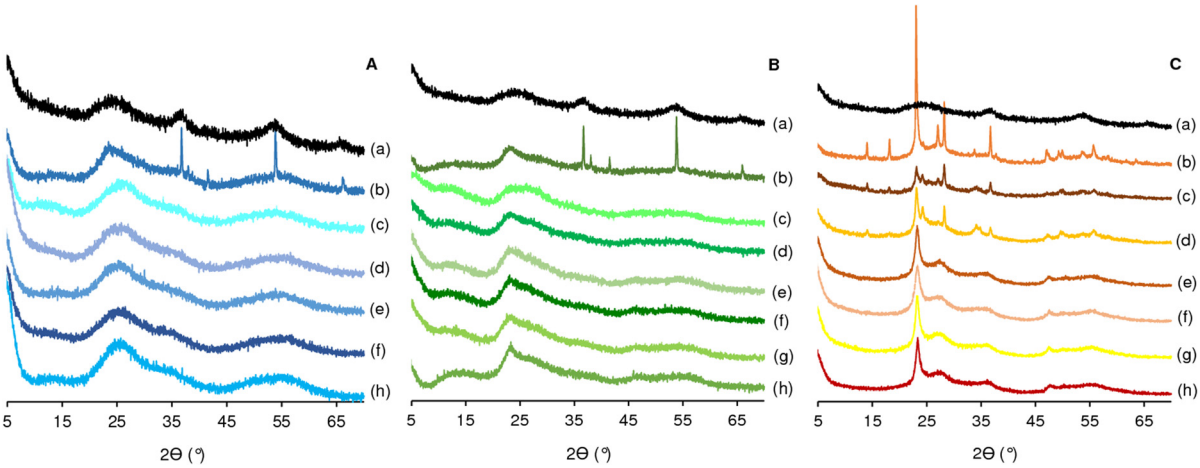

Fig. 1 PXRD patterns of the Mo,M oxides with M = Ta (A), Nb (B), or W (C): (b) Mo(50D)M-24, (c) Mo(75D)M-0.3, (d) Mo(50D)M-0.3, (e) Mo(50P)M-0.3, (f) Mo(25D)M-0.3, (g) Mo(25P)M-0.3 (excluding for M = Ta). For comparison, bulk (a) MoO_2 (A–C) and (h) M_xO_y (M = Ta (A), Nb (B), W (C)).

ICP-OES gave roughly comparable results to EDS (please see Table S1 and Fig. S2,† for selected materials).

Structural and morphological features. Fig. 1 shows the PXRD patterns of the prepared materials. The type of Mo precursor (D = MoO_2Cl_2, P = $MoCl_5$) did not considerably influence the structural features, as verified by comparing the materials Mo(*x*D)M-0.3 *versus* Mo(*x*P)M-0.3 with the same M and *x*.

The PXRD pattern of monometallic MoO_2 exhibits very broad reflections, which are indicative of the presence of very small crystallites. A 10-fold amplification of the diffractogram of MoO_2 showed very weak peaks centered at *ca.* 37, 54 and 66° 2θ (Fig. S3†), assignable to the (100), (102) and (110) crystal planes, respectively, of the hexagonal phase of molybdenum(IV) dioxide (ICDD PDF card no. 00-050-0739).[43] Koziej *et al.*[25] reported the solvothermal synthesis of MoO_2 nanoparticles possessing hexagonal crystal structure, using MoO_2Cl_2 as precursor and a solvent mixture of acetophenone and benzyl alcohol at 200 °C for 10 min (in the present study, solely acetophenone was used as solvent at 220 °C). Commercial molybdenum(VI) trioxide (MoO_3-com) possessed an orthorhombic crystal structure (ICDD PDF card no. 01-074-7909).

The PXRD patterns of Ta_2O_5, Nb_2O_5, Mo,Nb and Mo,Ta oxides resultant from solvothermal syntheses with a duration of *t* = 0.3 h, also show broad reflections indicative of small crystallites (Fig. 1A and B).

For the Mo,M oxides with M = Ta, Nb (*x* = 50), increasing the synthesis time from 0.3 h to 24 h led to the appearance of narrow reflections from the hexagonal MoO_2 phase (*ca.* 36.7, 38, 41.5, 53.8, 66° 2θ; ICDD PDF card no. 00-050-0739). This suggests that increasing the synthesis time resulted in the growth of the MoO_2 particles, but not of those of Ta_2O_5 or Nb_2O_5. It is worth noting that the presence of MoO_2 in the Mo, M oxides indicates that they may possess reduced Mo(IV) sites.

The PXRD pattern of the W oxide nanoparticles showed a main peak at *ca.* 24° 2θ, and additional weak broad peaks centered at *ca.* 27.4, 36, 47.6 and (very weak) 56° 2θ, assignable to $WO_{2.72}$ with monoclinic crystal structure (ICDD PDF card no. 04-005-4539) (Fig. 1C).

The Mo,W oxides Mo(*x*P)W-0.3 (*x* = 25, 50) and Mo(25D)W-0.3 exhibited comparable PXRD patterns to $WO_{2.72}$. For the remaining materials (with greater *x* and/or *t* values, using the D precursor), namely Mo(50D)W-0.3, Mo(75D)W-0.3 and Mo(50D)W-24, the peaks become more intense and narrower, suggesting particle growth. Besides $WO_{2.72}$, these materials seem to possess the orthorhombic phase of $(W_{1-x}Mo_x)O_3$ ($x \leq 1$; based on ICDD PDF card numbers 00-054-1012 and 00-046-1048); peaks at *ca.* 14, 18.2, 23, 27, 28.2 (main peak), 36.7, 47.1, 49.3, 50, 53.7, 55.7° 2θ. A longer synthesis time of 24 h (Mo(50D)W-24) led to enhanced crystallinity.

The morphology was studied by electron microscopy for selected materials, namely Mo(75D)M-0.3 and Mo(50D)M-24 with M = Ta, Nb or W, which were synthesised using the highest $(Mo/M)_{Syn}$ of 3 or longer synthesis time of 24 h, respectively (Fig. 2 and 3). The TEM, HAADF-STEM, and

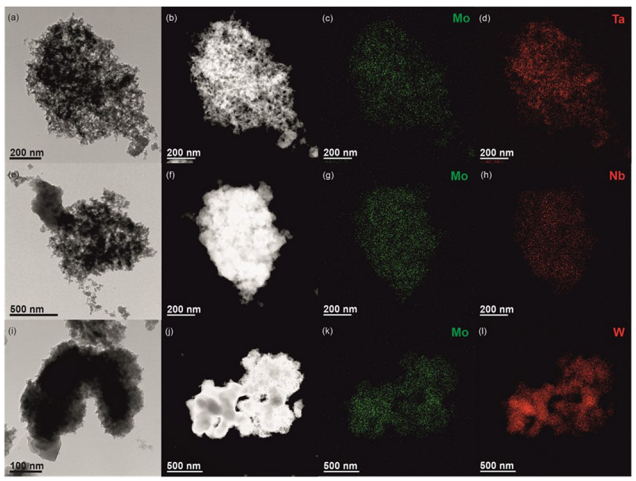

Fig. 2 TEM (a, e and i), HAADF-STEM and elemental maps (b–d, f–h and j–l) of Mo(75D)M-0.3 with M = Ta (a–d), Nb (e–h) or W (i–l).

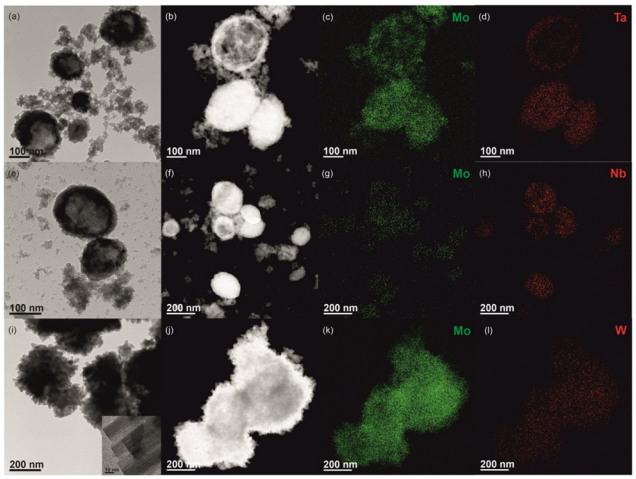

Fig. 3 TEM (a, e and i), HAADF-STEM and elemental maps (b–d, f–h and j–l) of Mo(50D)M-24 with M = Ta (a–d), Nb (e–h) or W (i–l). The inset in (i) shows a HRTEM image of the $WO_{2.72}$ nanobelts.

elemental maps showed that the materials consisted of agglomerates of intimately mixed nanoparticles of different morphology. For Mo,M oxides with t = 0.3 h, the Ta and Nb oxide components consist of irregular platelet-like nanoparticles with the size of *ca.* 19 nm and 3–5 nm, respectively; the W oxide component consists of agglomerated nanobelts of *ca.* 7–12 nm width; and the Mo oxide component is made of relatively large layered-like particles of *ca.* 57 nm. For t = 24 h, the Ta and Nb oxide components tend to form spherical agglomerates (Fig. 3(a, b, e and f)) of particles with sizes about 25 nm and 5–7 nm, respectively; the width of the W oxide nanobelts increases to *ca.* 25 nm, as well as their crystallinity (Fig. 3(i)); and the Mo oxide component becomes made of irregularly shaped interconnected particles of about 23 nm size. In general, elemental mapping suggested that the different particles are well mixed and in close proximity at the nanoscale (Fig. 2 and 3 and S4†). The pure MoO_2 sample consists of large sphere-like particles in the size range 350 to 500 nm.

Textural properties. The M_xO_y and Mo,M oxide materials possessed higher S_{BET} than bulk MoO_2 (44 $m^2\ g^{-1}$), (Table S2†). The S_{BET} values for M_xO_y were intermediate of those of the respective Mo,M oxides (with the same M); specifically, S_{BET} = 268 $m^2\ g^{-1}$ for Nb_2O_5 compared to 193–402 $m^2\ g^{-1}$ for the Mo,Nb oxides; 126 $m^2\ g^{-1}$ for Ta_2O_5 compared to 54–278 $m^2\ g^{-1}$ for the Mo,Ta oxides; and 185 $m^2\ g^{-1}$ for $WO_{2.72}$ compared to 97–214 $m^2\ g^{-1}$ for the Mo,W oxides.

Regarding the type of Mo precursor, for the materials Mo(xD)M-0.3 with the same M and synthesized using the D precursor, S_{BET} decreased with increasing Mo/M ratio of the materials (Fig. S5(a)†), whereas the opposite was verified for the related materials synthesized using the P precursor (Fig. S5(b)†). Hence, S_{BET} does not solely depend on the type of Mo precursor (or Mo/M) and may be due to interplay of different factors. The type of M metal may also influence S_{BET}; *e.g.*, Mo(50D)M-24 possessing (different) M = Ta and Nb, and synthesized using the same D precursor, possessed somewhat comparable PXRD features (Fig. 1) and chemical compositions (Table S1†), albeit considerably different S_{BET} (54 and 402 $m^2\ g^{-1}$, M = Ta and Nb, respectively). Possible differences in the size/density/structure of the nanoparticle ensembles or agglomerates,[44,45] may at least partly influence the interparticle void space and total specific surface area. For example, for the Mo(50D)M-0.3 family, S_{BET} (Table S2†) increased with decreasing particle size: M = Ta (19 nm width; 98 $m^2\ g^{-1}$); M = W (7–12 nm; 118 $m^2\ g^{-1}$); M = Nb (3–5 nm; 254 $m^2\ g^{-1}$). On the other hand, the morphology also seems to affect S_{BET}; *e.g.*, particle sizes were slightly larger for Mo(50D)Nb-24 than (morphologically different) Mo(50D)Nb-0.3, but the former possessed higher S_{BET} (402 $m^2\ g^{-1}$ *versus* 254 $m^2\ g^{-1}$).

Surface chemistry. In general, the ATR FT-IR spectra of the Mo,M oxides with M = Ta, Nb, resembled somewhat closer the spectral features of the corresponding monometallic materials M_xO_y than of MoO_2 (Fig. 4). MoO_2 exhibited a relatively intense IR band at *ca.* 956 cm^{-1} due to vibrational modes of terminal Mo=O groups, and a broad band centred at *ca.* 660 cm^{-1} which may be associated with polynuclear Mo–O–Mo groups.[46–48]

Bulk Nb_2O_5 exhibited a poorly defined spectrum; a broad band centred at *ca.* 875 cm^{-1} may be due to stretching vibrations of Nb=O groups (Fig. 4B).[49] Ta_2O_5 exhibited several broad bands below 1000 cm^{-1} (Fig. 4A), which may be due to vibrational modes of Ta–O–Ta and Ta–O type groups with different bond lengths/angles/chemical environments (band assignments are not consensual in the literature).[50–56] A comparative study for the Mo,M oxides with M = Ta, Nb, indicated that an absorption band at *ca.* 956 cm^{-1} (assignable to ν(Mo=O)) was distinguishable for Mo(75D)M-0.3 (M = Ta, Nb) and Mo(50D)Ta-24 and hardly distinguishable for the remaining materials (Fig. 4(A and B)). A broad band centred at *ca.* 660 cm^{-1} (assignable to polynuclear Mo–O–Mo) was somewhat distinguishable for Mo,Ta oxides, and not clearly distinguishable for the Mo,Nb-mixed oxides (possibly due to overlapping of broad bands).

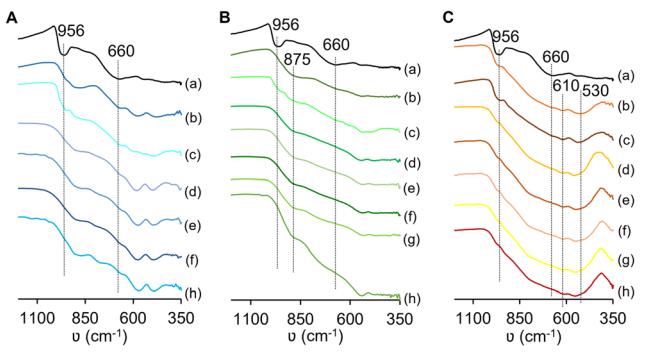

Fig. 4 ATR FT-IR spectra of the materials possessing M = Ta (A), Nb (B), or W (C) and, for comparison, (a) MoO_2 is included in the three plots; (b) Mo(50D)M-24, (c) Mo(75D)M-0.3, (d) Mo(50D)M-0.3, (e) Mo(50P)M-0.3, (f) Mo(25D)M-0.3, (g) Mo(25P)M-0.3 (excluding for M = Ta) and (h) M_xO_y (M = Ta (A), Nb (B), W (C)).

Regarding the tungsten-based materials, $WO_{2.72}$ exhibited poorly defined bands at *ca.* 956, 610 and 530 cm^{-1} (Fig. 4(C)). The first band may be due to terminal W═O groups[57] and the others to polynuclear W–O–W groups possessing different bond lengths/angles/chemical environments.[57,58] Similarly, the Mo,W oxides exhibited a band at *ca.* 956 cm^{-1} assignable to ν(M═O) (M = Mo or W), and bands at *ca.* 610 and 530 cm^{-1}. The band at *ca.* 660 cm^{-1}, associated with polynuclear Mo–O–Mo groups (verified for monometallic MoO_2), was not clearly distinguishable in the spectra of the Mo,W oxides.

The M metals belong to group 5 (Nb, Ta) and 6 (W), and were in their highest oxidation states in the corresponding synthesis precursors (Nb(v), Ta(v), W(vi)). The metals in these oxidation states may be present in the Mo,M oxides (*e.g.*, group 5 metals may be less prone to changes in oxidation state). On the other hand, molybdenum (group 6) may have different oxidation states. DR UV-vis spectroscopy may give insights into the coordination numbers and oxidation states of the metal sites. Fig. S6† shows the DR UV-vis spectra of the materials M_xO_y, MoO_2 and selected Mo,M oxides, namely Mo(75D)M-0.3 and Mo(50D)M-24 (M = Ta, Nb, W). In general, the mixed metal oxides exhibited bands centred at *ca.* 210–215, 240–250 and 310–320 nm. Rigorous assignments of these bands are difficult, partly due to possible superimposable contributions from M and/or Mo containing groups. Some literature studies suggested that bands below *ca.* 250 nm may be due to isolated molybdenum sites,[59–62] albeit (polymeric) MoO_2 also exhibited bands at *ca.* 215 and 240 nm, which were also verified for Ta_2O_5, Nb_2O_5 and $WO_{2.72}$. Different literature studies suggested that bands below *ca.* 250 nm may be partly due to distorted four-coordinated {TO_4} sites (T = Mo or M);[59–61,63,64,67–71] In the cases of MoO_2 and Mo,M oxides (for which PXRD identified the presence of MoO_2), the bands below 250 nm may be associated with reduced Mo(iv) groups. The relatively low oxidation state of molybdenum in MoO_2 (Mo(iv)) results in an increasing absorption above 350 nm, which was also verified for crystalline (commercial) MoO_2-com (together with very weak absorptions at *ca.* 210 and 240 nm, Fig. S6D†) and in agreement with literature data.[60,70–73] The presence of Mo(iv) sites in the Mo,M oxide nanomaterials was further supported by the fact that the very dark color of MoO_2 and MoO_2-com was also verified for the Mo,M oxides, especially Mo(75D)M-0.3 and Mo(50D)M-24.

The nanomaterials Nb_2O_5 and $WO_{2.72}$ exhibited a band centered at *ca.* 320 nm which may be partly due to six-coordinated metal sites.[63,65,67,74] The Mo,M oxides (M = Ta, Nb, W) also exhibited a band at *ca.* 310–330 nm, which at least for the Mo,Ta oxides may be attributed to molybdenum containing groups (*e.g.*, six-coordinated Mo(vi) sites or Mo–O–Mo groups),[59–62,70,75,76] because Ta_2O_5 did not exhibit bands in this spectral range. In relation to the defective nanomaterials, crystalline (commercial) MoO_3-com (Mo(vi)), Nb_2O_5-com (Nb(v)) and WO_3-com (W(vi)) exhibited a higher wavelength band (*ca.* 355 nm) which may be associated with their infinitely (long range ordered) stacked octahedra of Mo(vi), Nb(v) and W(vi), respectively (Fig. S6-D†).[71,75,77–79] A lower wavelength band (*ca.* 260 nm) was predominant for crystalline Ta_2O_5-com which may be associated with its distinct coordination features (shared distorted polyhedra of Ta(v), *i.e.*, {TaO_6} octahedra and {TaO_7} pentagonal bipyramides).[66,69] In summary, the above results suggested that decreasing the particle sizes down to the nanoscale influences the surface chemistry, and the nanomaterials may possess molybdenum sites with different oxidation states (*e.g.*, Mo(iv), Mo(vi)).

Catalytic studies

General considerations. The influence of the material properties on the catalytic performances of the metal oxides and catalyst benchmarking was firstly investigated, based on the model reaction of *cis*-cyclooctene (Cy) with *tert*-butylhydroperoxide (TBHP) (for catalyst screening).

TFT was chosen as solvent since it is readily available, relatively inexpensive, and has good capacity to dissolve a wide range of organic compounds.[80] Its relatively high boiling point (*ca.* 102 °C) makes it more appealing (*e.g.*, avoiding atmospheric emissions) than other more volatile halogenated solvents. Additionally, its poor coordinating properties avoids competitive reactions with reactant molecules in the coordination to active metal species, which, together with the remaining aspects, has contributed to its successful use as solvent in several catalytic epoxidation systems.[81,82]

Cyclooctene oxide (CyO) was the sole product (100% selectivity), formed in up to 100% yield within 24 h, at 70 °C. Blank tests carried out without catalyst or without oxidant, gave negligible olefin conversion.

The bulk M_xO_y materials led to sluggish results; conversion at 24 h was 25%, 7% and 4% for M = Nb, Ta and W, respectively. On the other hand, MoO_2 led to 100% conversion at 1 h, suggesting that molybdenum plays an important catalytic role. According to the literature, the performance of molybdenum oxides may strongly depend on the type of crystalline structure.[83] For example, commercial orthorhombic MoO_3-com (Fig. S7†) was far less active (conversion at 1 h/4 h/24 h was 33%/79%/100%) than MoO_2. However, MoO_2 presents stability issues; the hexagonal crystal structure may suffer phase transition;[25,84] and the epoxidation reaction in the presence of MoO_2 led to yellow-coloured liquid phase, characteristic of soluble oxidized molybdenum species. This was further confirmed by a catalyst filtration test, which indicated a major homogeneous catalytic contribution (please see the ESI† for details).

Based on the mechanistic studies reported in the literature for Mo-catalysed EPO of olefins with hydroperoxide oxidants (ROOH), the active oxidizing species may be formed *via* a heterolytic mechanism involving the coordination of the oxidant (ROOH) to a molybdenum centre.[85–88] This leads to the formation of a moiety of the type {Mo-OOR} responsible for the oxygen atom transfer step to the olefin, giving the epoxide product (plus the

coproduct of TBHP, namely *tert*-butanol). These mechanistic considerations may also apply for W-catalysed olefin epoxidation,[89–92] and other metals (*e.g.*, active oxidizing species possessing the moiety {M-OOR} were reported for Ta-containing catalysts in olefin epoxidation[93]). Hence, one cannot exclude the possible roles of Mo and M sites of the Mo,M oxides, as discussed below.

Influence of materials synthesis conditions on the catalytic performance. Based on the characterisation studies, the type of Mo precursor (P or D), synthesis time (t), mole ratio $(Mo/M)_{Syn}$ of the synthesis mixture and type of M metal, influenced the material properties, which may affect the catalytic performances.

Concerning the type of Mo precursor (keeping constant the type of M), the Mo,M oxides synthesized using MoO_2Cl_2 (D) were, in general, more active than those synthesized using $MoCl_5$ (P), under similar conditions (Fig. 5(a–c)); exceptionally, Mo(50D)Ta-0.3 and Mo(50P)Ta-0.3 possessed somewhat comparable activities.

The influence of x (or $(Mo/M)_{Syn}$) was investigated for the two families of materials Mo(xP)M-0.3 and Mo(xD)M-0.3, keeping constant the type of Mo precursor, type of M metal and synthesis time (t = 0.3 h) (Fig. 5(d–f) and S8†). In general, olefin conversion (Fig. 5(d–f)) and initial activity (Fig. S8†) increased with increasing x. For example, for the Mo(xD)M-0.3 family (Fig. S8(a)†), initial activity for M = Ta increased from 18 $mmol_{Cy}\ g_{cat}^{-1}\ h^{-1}$ (x = 25) to 157 $mmol_{Cy}\ g_{cat}^{-1}\ h^{-1}$ (x = 75); for M = Nb, from 25 $mmol_{Cy}\ g_{cat}^{-1}\ h^{-1}$ (x = 25) to 157 $mmol_{Cy}\ g_{cat}^{-1}\ h^{-1}$ (x = 75); and for M = W, from 27 $mmol_{Cy}\ g_{cat}^{-1}\ h^{-1}$ (x = 25) to 157 $mmol_{Cy}\ g_{cat}^{-1}\ h^{-1}$ (x = 75). The

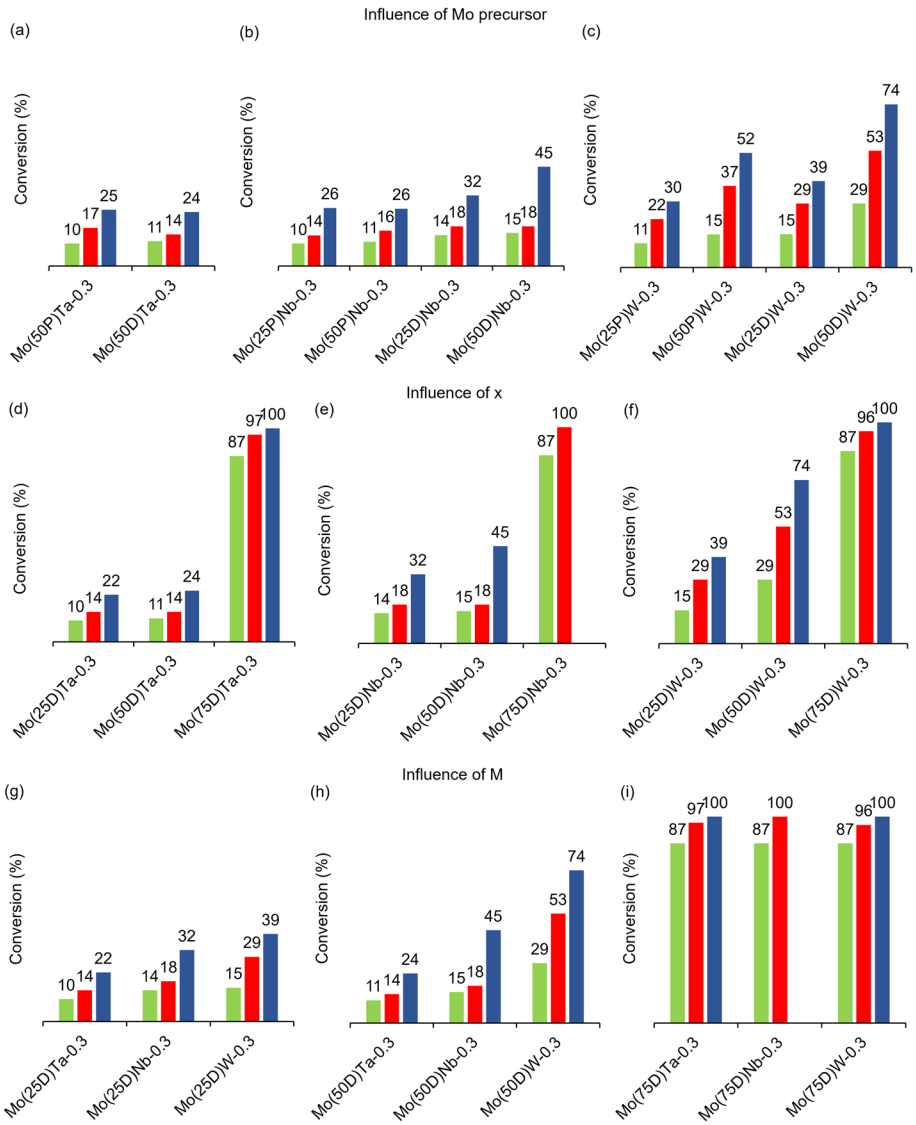

Fig. 5 Influence of the material synthesis conditions on the catalytic performances: type of Mo precursor ((a) Mo,Ta oxides, (b) Mo,Nb oxides, (c) Mo,W oxides); relative amount of Mo (x) in the material synthesis mixture ((d) Mo,Ta oxides; (e) Mo,Nb oxides; (f) Mo,W oxides); and type of M metal (Mo(xD)M-0.3 with x = 25 (g), 50 (h) or 75 (i)). Reaction conditions: mole ratio TBHP : Cy = 1.5, 5.6 $g_{cat}\ mol_{Cy}^{-1}$, 70 °C. Each set of three bars indicates Cy conversion at 1 h (green), 4 h (red) or 24 h (blue) reaction. Epoxide (CyO) selectivity was always 100%.

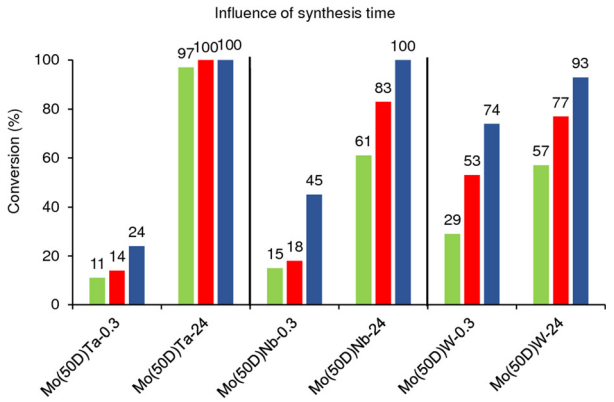

Fig. 6 Influence of the material synthesis time (0.3 h or 24 h) on the performances of the Mo(50D)M catalysts. Reaction conditions: mole ratio TBHP : Cy = 1.5, 5.6 g_{cat} mol_{Cy}^{-1}, 70 °C. Each set of three bars indicates Cy conversion at 1 h (green), 4 h (red) or 24 h (blue) reaction. Epoxide (CyO) selectivity was always 100%.

highest conversion at 1 h was 87%, reached for the materials with x = 75 (Fig. 5(d–f)).

On the other hand, increasing the synthesis time from 0.3 h to 24 h (*i.e.*, Mo(50D)M-0.3 *versus* Mo(50D)M-0.24 with the same M) favoured the epoxidation reaction kinetics (Fig. 6). The differences in reaction kinetics were very pronounced, especially for M = Ta (for the material synthesis time of t = 0.3 h and 24 h, the conversion was 14 and 100%, respectively, at 4 h). Initial activity increased from 20 $mmol_{Cy}$ g_{cat}^{-1} h^{-1} (t = 0.3 h) to 175 $mmol_{Cy}$ g_{cat}^{-1} h^{-1} (t = 24 h) for M = Ta; from 27 $mmol_{Cy}$ g_{cat}^{-1} h^{-1} (t = 0.3 h) to 110 $mmol_{Cy}$ g_{cat}^{-1} h^{-1} (t = 24 h) for M = Nb; and from 52 $mmol_{Cy}$ g_{cat}^{-1} h^{-1} (t = 0.3 h) to 103 $mmol_{Cy}$ g_{cat}^{-1} h^{-1} (t = 24 h) for M = W (Fig. S9†).

In general, based on the characterisation studies for the materials with the same M metal, increasing x and t led to higher Mo/M of the materials formed, which may partly explain the faster catalytic reaction kinetics, as shown in Fig. 7, *i.e.*, conversion somewhat increased with Mo/M, especially for Mo/M > 0.1.

Concerning the influence of the type of M metal, a comparative study for the materials Mo(xD)M-0.3 with the same x, indicated differences in catalytic activities. Specifically, for x = 25 or 50, olefin conversion (Fig. 5(g–i)) and initial activity (Fig. S10†) increased in the order Ta < Nb < W. For x = 75, the differences in catalytic results were not pronounced because of the very high activity of these materials (*ca.* 87% conversion at 1 h, and initial activity = 157 $mmol_{Cy}$ g_{cat}^{-1} h^{-1} for the three materials Mo(75D)M-0.3). These results did not correlate directly with S_{BET} which increased in the order Ta (78 m^2 g^{-1}) < W (104 m^2 g^{-1}) < Nb (222 m^2 g^{-1}) (Table S2†).

In order to gain further insight into the influence of the type of M, a comparative study was carried out for the Mo(50D)M-0.3 materials, keeping constant the initial mole ratio Mo : olefin of the catalytic reaction mixture (Fig. S11†). If all the molybdenum sites of the different catalysts were equivalent (*i.e.*, possessing equal intrinsic activity), one could expect the reaction rate to be similar because the initial mole ratio Mo : olefin was kept constant in these catalytic tests. However, this was not the case, *i.e.*, the initial activity followed the order Nb < Ta < W and the conversion at 24 h followed the order Ta < Nb < W, indicating differences in reaction kinetics, and suggesting that not all Mo sites were equivalent. The characterisation studies of the materials with different M, indicated structural differences, *e.g.*, Mo(50D)W-0.3 is crystalline, whereas the corresponding materials with M = Ta and Nb did not exhibit distinguishable crystalline domains (Fig. 1). Additionally, the characterisation studies suggested that the nanomaterials may possess different types of Mo sites (non-equivalent sites), which may have different intrinsic activities. Moreover, the coordination environment and/or redox properties of M species may be different; *e.g.*, according to the literature, Ta and Nb with similar coordination spheres may possess significantly different redox properties.[94] From the characterization studies of the MoM oxides, one cannot exclude the possible existence of proximal Mo and M species. Accordingly, the M species could influence the electronic/structural features of vicinal Mo species, and consequently the intrinsic activities. Overall, the catalytic performances seem to be due to a complex interplay of different material properties, such as structure, surface chemistry and composition.

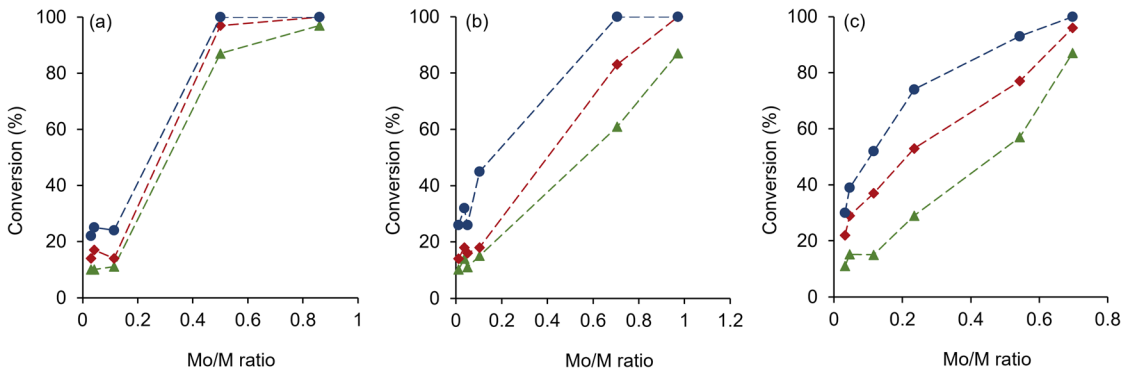

Fig. 7 Dependency of Cy conversion at 1 h (Δ), 4 h (◊) or 24 h (○) reaction, on the Mo/M ratio (EDS) of the Mo,M oxides with M = Ta (a), Nb (b) or W (c). Reaction conditions: mole ratio TBHP : Cy = 1.5, 5.6 g_{cat} mol_{Cy}^{-1}, 70 °C. Epoxide (CyO) selectivity was always 100%.

Catalyst stability. The catalytic stability was studied for the families of materials with the highest catalytic activities, namely Mo(75D)M-0.3 and Mo(50D)M-24. These solids were reused in consecutive batch runs (Fig. S12†), keeping constant the initial mass ratio of Cy : TBHP : catalyst, and characterized after use. In general, the olefin conversion remained roughly comparable in consecutive runs, excluding the materials with M = Ta which suffered partial drop of activity (*e.g.*, for Mo(50D)Ta-24, conversion at 4 h decreased from 100% in run 1 to 75% in run 3; Fig. S12(a)†).

The characterisation studies of the used Mo,M catalysts indicated that, in general, their structural (PXRD, Fig. S13†) and morphological features (electron microscopy, Fig. S14–S17†), metal distributions (elemental mappings, Fig. S14 and S15†), chemical compositions (Mo : M ratio, Fig. S18†) and surface chemistry (ATR FT-IR (Fig. S19†) and DR UV-vis (Fig. S20†) spectroscopy) were essentially preserved. Exceptionally, the MoO_2 hexagonal phase remained present in Mo(50D)Nb-24-used, but not in Mo(50D)Ta-24-used (Fig. S13†), which may be due to an interplay of several factors such as stability issues. MoO_2 nanoparticles may be susceptible to partial oxidation of interfacial Mo(IV) sites,[95–97] and small variations in the molybdenum valence may affect the physical properties.[83] Accordingly, differences in redox properties and coordination features of Ta and Nb sites (discussed in the literature for different coordination compounds of these metals[94,98]) may have implications on the stability of immobilized MoO_2.

Epoxidation of biobased FAMEs. Among the most abundant fatty acids are the unsaturated C18 compounds oleic, linoleic and linolenic acids (and respective esters).[11] Three of the best performing catalysts, namely Mo(75D)M-0.3 with M = Ta, Nb and W, were further explored for the epoxidation of methyl oleate (MeOle) and methyl linoleate (MeLin) as model substrates of FAMEs, at 70 °C (Scheme 1). These materials effectively promoted the epoxidation of the FAMEs (Fig. 8 and 9, Table 1), leading to conversions in the range 84–95% and 97–100% for MeOle and MeLin, respectively, at 24 h. The higher reactivity of MeLin than MeOle (keeping constant the initial mole ratio of oxidant/

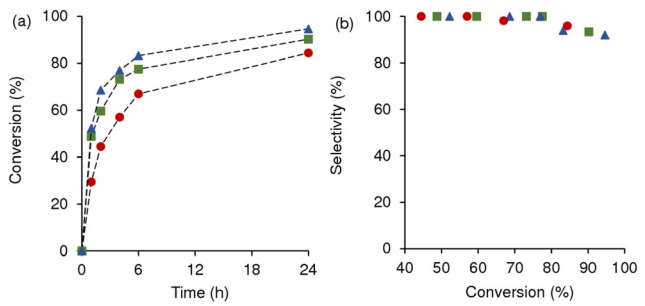

Fig. 8 Epoxidation of methyl oleate (MeOle) with TBHP, at 70 °C, in the presence of Mo(75D)M-0.3 with M = Ta (○), M = Nb (Δ) and M = W (□): (a) kinetic profiles and (b) dependency of product selectivity on conversion for the monoepoxide. Reaction conditions: mole ratio TBHP : FAME = 1.5, 5.6 g_{cat} mol_{FAME}^{-1}, 70 °C.

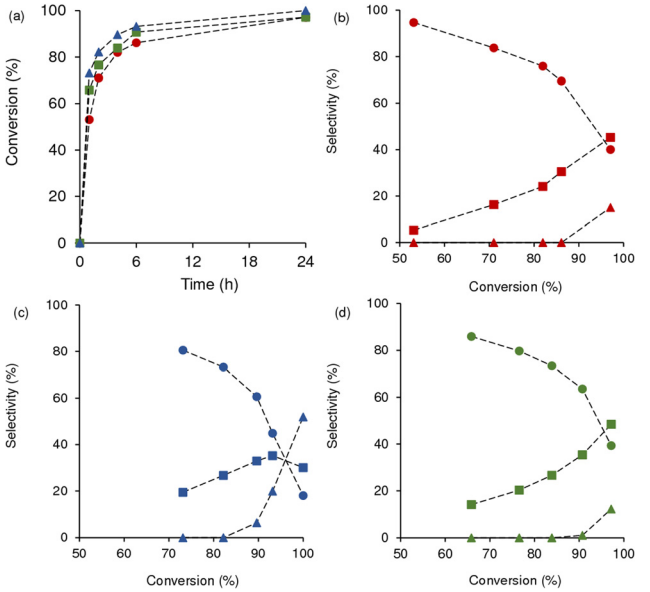

Fig. 9 (a) Kinetic profiles of methyl linoleate (MeLin) epoxidation, in the presence of Mo(75D)M-0.3 with M = Ta (○), M = Nb (Δ) and M = W (□), and (b–d) dependency of selectivity on conversion (monoepoxides (○), diepoxides (□) and furan type products (Δ)). Reaction conditions: mole ratio TBHP : FAME = 2.5, 5.6 g_{cat} mol_{FAME}^{-1}, 70 °C.

(C=C double bond)), parallels that reported in the literature for Nb-silica catalysts (although for the latter, olefin conversion tended to a plateau after *ca.* 1 h reaction at 90 °C due to partial catalytic deactivation[99]). Since MeLin is a polyunsaturated olefin, its conversion may be faster (two C=C double bonds are available) than of the monoene MeOle. Moreover, it was proposed in the literature that polyunsaturated FAMEs may be more reactive than monounsaturated ones, due to possible electron-donating effects of adjacent allyl groups (H_2C=CH–CH_2).[100]

For each FAME, the initial catalytic activity (mmol g_{cat}^{-1} h^{-1}) followed the order Nb (94 $mmol_{MeOle}$ g_{cat}^{-1} h^{-1}; 132 $mmol_{MeLin}$ g_{cat}^{-1} h^{-1}) > W (88 $mmol_{MeOle}$ g_{cat}^{-1} h^{-1}; 119 $mmol_{MeLin}$ g_{cat}^{-1} h^{-1}) > Ta (69 $mmol_{MeOle}$ g_{cat}^{-1} h^{-1}; 96 $mmol_{MeLin}$ g_{cat}^{-1} h^{-1}). These results somewhat correlated with the Mo/M ratio which decreased in the same order (Fig. 8 and 9, Table S1†), and with decreasing specific surface area (222 m^2 g^{-1} (M = Nb) > 104 m^2 g^{-1} (M = W) > 78 m^2 g^{-1} (M = Ta), Table S2†). However, the initial activities expressed per unit of surface area (mmol m^{-2} h^{-1}) followed a different trend: Nb (0.42 $mmol_{MeOle}$ m^{-2} h^{-1}; 0.59 $mmol_{MeLin}$ m^{-2} h^{-1}) < W (0.85 $mmol_{MeOle}$ m^{-2} h^{-1}; 1.14 $mmol_{MeLin}$ m^{-2} h^{-1}) ≅ Ta (0.88 $mmol_{MeOle}$ m^{-2}; 1.23 $mmol_{MeLin}$ m^{-2} h^{-1}). Possibly, the catalytic activity may be partly influenced by the density of active sites.

The MeOle reaction in the presence of Mo(75D)M-0.3 gave mainly the epoxide product, methyl 9,10-epoxyoctadecanoate (MeOleEp) (Scheme 1), formed in 96% selectivity at 84% conversion for M = Ta, and 92–93% selectivity at 90–95% conversion for M = Nb and W (Fig. 8, Table 1).

The reaction of MeLin gave mono- and diepoxides (Fig. 9, Scheme 2). The monoepoxides were methyl 12,13-epoxy-9*Z*-

Table 1 Selected catalytic results of FAMEs EPO, in the presence of Mo(75D)M-0.3

	Reaction conditions[a]					
M	FAME	*t*/h	Conv.[b] (%)	Product[c]	Select.[d] (%)	Yield[d] (%)
Ta	MeOle	6	67	MeOleEp	98	66
		24	84		96	81
Nb		6	83	MeOleEp	94	78
		24	95		92	87
W		6	78	MeOleEp	100	78
		24	90		93	84
Ta	MeLin	6	86	MeLinEp	70	60
				MeLinDiEp	30	26
				CFur	0	0
		24	97	MeLinEp	40	39
				MeLinDiEp	45	44
				CFur	15	15
Nb		6	93	MeLinEp	45	42
				MeLinDiEp	35	33
				CFur	20	19
		24	100	MeLinEp	18	18
				MeLinDiEp	30	30
				CFur	52	52
W		6	91	MeLinEp	64	58
				MeLinDiEp	35	32
				CFur	1	1
		24	97	MeLinEp	40	39
				MeLinDiEp	48	47
				CFur	12	12
Nb[e]		6	93	MeLinEp	20[e]	20[e]
				MeLinDiEp	61[e]	61[e]
				CFur	19[e]	19[e]
		24	100	MeLinEp	8[e]	8[e]
				MeLinDiEp	64[e]	64[e]
				CFur	28[e]	28[e]

[a] Reaction conditions: mole ratio TBHP : FAME = 1.5 for MeOle or 2.5 for MeLin, 5.6 g_{cat} mol_{FAME}^{-1}, 70 °C. [b] Olefin conversion at the specified reaction time (*t*). [c] MeOleEp = methyl 9,10-epoxyoctadecanoate, MeLinEp = methyl 9,10-epoxy-12-octadecenoate and methyl 12,13-epoxy-9-octadecenoate, MeLinDiEp = methyl 9,10-12,13-diepoxyoctadecanoate, CFur = furan type cyclic products. [d] Selectivity or yield of products, at 6 h/24 h. [e] Reaction performed at 90 °C.

octadecanoate and methyl 9,10-epoxy-12*Z*-octadecanoate (MeLinEp), and the diepoxides were diastereoisomers of methyl 9,10,12,13-diepoxy-octadecanoate (MeLinDiEp). The selectivity to the total epoxides (MeLinEp plus MeLinDiEp) at 6 h/24 h reaction was 99%/88% at 91%/97% conversion for M = W; 100%/85% at 86%/97% conversion for M = Ta; and 80%/48% at 93%/100% conversion for M = Nb.

For the three catalysts with MeLin, the monoepoxides were formed in approximately equimolar amounts (negligible regioselectivity), suggesting that the two C=C double bonds are similarly reactive. The kinetic profiles suggest that the monoepoxides are intermediates of the conversion of MeLin to diepoxides (Scheme 2). The latter are converted to (cyclic) furan type products (CFur), namely methyl 10,13-dihydroxy-9,12-epoxy-octadecanoate and methyl 9,12-dihydroxy-10,13-epoxy-octadecanoate. According to the literature, these furan type products may be formed *via* acid-catalyzed ring opening of one epoxide group (giving diol intermediates) and subsequent cyclisation involving the other epoxide group.[42,101,102] However, diol intermediates were not detected in measurable amounts under these conditions, suggesting that their cyclisation may be relatively fast.

For Mo(75D)Ta-0.3 and Mo(75D)W-0.3, the product distributions at 24 h were very similar: at 97% MeLin conversion, the selectivities were 40% MeLinEp, 45–48% MeLinDiEp and 12–15% CFur (Fig. 9, Table 1). The Mo(75D)Nb-0.3 catalyst led to higher CFur selectivity; 52% selectivity, compared to 18% and 30% selectivity to mono and diepoxides, respectively, at 100% conversion, 24 h. Although the latter material possessed higher S_{BET}, which may be favorable for the adsorption of intermediates and corresponding consecutive reactions, this does not seem to be the sole factor influencing the products distribution because no direct correlation between S_{BET} and the product distributions (for the different materials) could be established. The differences in product distributions may be partly associated with differences in structure/electronic properties of the materials' active sites (suggested by the characterization studies). On the other hand, water (TBHP may contain up to 4 wt% water) may interact with metal sites and induce the formation of Brønsted acidity,[103] which may contribute to epoxide ring opening reactions. Moreover, according to the literature, *in situ* water adsorption may affect the coordination number and oxidation state of molybdenum.[71]

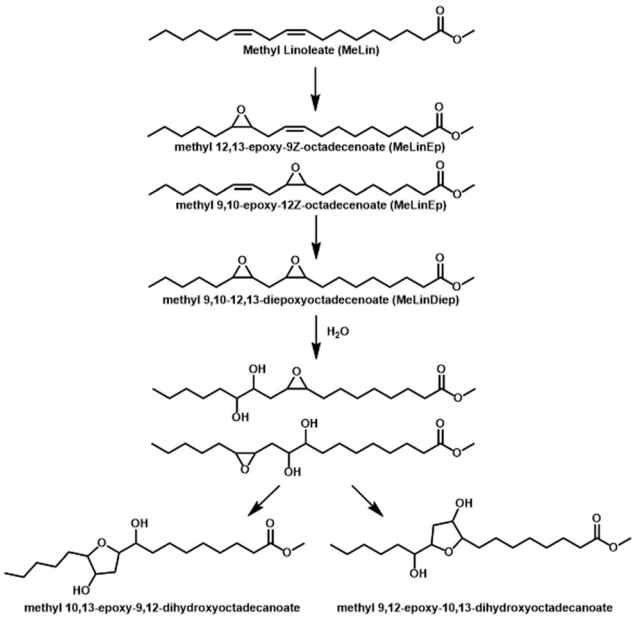

Scheme 2 Conversion of methyl linoleate (MeLin) in the presence of Mo(75D)M-0.3 (M = W, Nb and Ta), leading to epoxides and furan type products.

Increasing the MeLin reaction temperature from 70 to 90 °C in the presence of Mo(75D)Nb-0.3, led to higher initial activity (increased from 132 to 170 $mmol_{MeLin}\ g_{cat}^{-1}\ h^{-1}$) and the reaction was complete within 4 h (Fig. S21†). Moreover, the ratio of diepoxides/monoepoxides was enhanced (*i.e.*, MeLinDiEp/MeLinEp = 64%/8%, at 24 h), as well as the ratio of (total epoxides)/CFur, (72%/28%). According to the above mechanistic considerations (conversion of epoxide to CFur *via* the intermediate formation of diol), the presence of water (which was added together with the oxidant) may cause epoxide ring opening. Possibly, at the higher reaction temperature, competitive adsorption effects may be unfavourable for water adsorption, avoiding consecutive reactions.

To gain further insights into the influence of water on the products distributions, the following catalytic tests were carried out for MeLin conversion, in the presence of Mo(75D) Nb-0.3, at 70 °C (Fig. S21†): (i) adding (dehydrated) molecular sieves to the reaction mixture (to reduce the water content in the liquid bulk); and (ii) adding water to the catalytic reaction mixture (*ca.* 35 wt% relative to the initial mass of MeLin). For test (i), CFur yield was lower (20% at 24 h) than for the normal catalytic test (52%), and MeLinDiEp yield was higher (57% MeLinDiEp yield at 24 h, compared to 30% for the normal catalytic test). Hence the removal of water enhanced diepoxides yields and was unfavorable for CFur formation. This was further confirmed by test (ii) which gave mainly CFur (87%/98% yield at 24 h/48 h), and MeLinDiEp was not formed in measurable amounts. In parallel to that verified for test (ii), the addition of water to the reaction of MeLin at 90 °C led to faster formation of CFur (88%/98% yield at 6 h/24 h, compared to 29%/55% at 24 h/48 h for the normal catalytic test at 90 °C) (Fig. S21†). Water may react with epoxides leading to ring-opening and formation of diol intermediates, and, as discussed above, the latter may undergo fast cyclisation to CFur.

To the best of our knowledge, these are the first Mo,M oxides (M = W, Nb or Ta) reported as catalysts for the target reactions. A literature survey for Mo-containing silica/silicates tested in the epoxidation of MeOle or MeLin, indicated two previous studies.[104,105] Gao *et al.*[105] reported the epoxidation of MeOle with H_2O_2, in the presence of molybdenum supported on the external surface of TS-1, which led to *ca.* 65% MeOleEp selectivity at *ca.* 52% conversion, 80 °C, 12 h; *e.g.*, Mo(75D)M-0.3 led to 100% MeOleEp selectivity at 78% conversion, 70 °C, 6 h (Table 1). In a different study, molybdenum containing mesoporous silica of the type TUD-1 led to 100% MeOleEp selectivity at 89% MeOle conversion, using TBHP as oxidant at 70 °C, 24 h.[104] The two literature studies reported deactivation of the silica-based catalysts.

A literature survey covering fully inorganic heterogeneous catalysts possessing different transition metals or oxide supports, tested for the target reactions is presented in Table S3.† There are few literature studies, and they are mostly focused on titanium-containing silicas/silicates. With MeOle as substrate, the results for Mo(75D)M-0.3 (entries 1–3) compared favorably to those reported for other catalysts. The highest epoxide yield was reported for MoO_3–Al_2O_3, albeit at a higher reaction temperature of 115 °C (99% MeOleEp yield) and catalytic stability was not reported (entry 4).[106] Ti–SiO_2 and Ti-MCM-41 led to 86% at 24 h and >95% at 12 h, respectively, at 90 °C (entries 7, 11), but catalytic stability was also not reported.[107] With MeLin as substrate, the yields of total epoxide products for the Mo(75D)M-0.3 catalysts were intermediate (entry 15) of those reported for Ti-silicas, albeit the catalytic stability was not reported.[107,108]

Conclusions

The challenge of developing selective, stable epoxidation solid catalysts for epoxidation (EPO) of relatively bulky olefins with relatively bulky *tert*-butylhydroperoxide under mild conditions, was studied by developing nanocatalysts consisting of Mo,M oxides (namely, Mo(*x*D)M-*t* and Mo(*x*P)M-*t* with M = Ta, Nb or W). The catalysts were synthesized *via* versatile solvothermal methodology, simply using the desired metals precursors and (biodegradable) acetophenone. In order to meet superior catalytic performances, the material synthesis conditions were optimised, namely, the type (D or P) and amount (*x*) of molybdenum precursor, type of M metal, and synthesis time (*t* = 0.3 or 24 h). The obtained Mo, M oxides possessed Mo/M ratios in the range 0.01–0.97, specific surface areas in the range 54–402 $m^2\ g^{-1}$ and different structural features. Catalytic screening tests (*cis*-cyclooctene model reaction) indicated that EPO activity and epoxide yields can be enhanced by: (i) using MoO_2Cl_2 (D) as Mo precursor instead of $MoCl_5$ (P), (ii) increasing the mole ratio $(Mo/M)_{Syn}$ of the synthesis mixture, and/or (iii)

increasing the synthesis time. Importantly, the catalysts Mo(75D)M-0.3 and Mo(50D)M-24 with M = Nb, W were the most stable.

The Mo(75D)M-0.3 nanocatalysts effectively promoted the EPO of relatively bulky biobased fatty acid methyl esters (methyl oleate, methyl linoleate) with TBHP; *e.g.*, Mo(75D)M-0.3 led to 92–96% epoxide selectivity at 84–95% methyl oleate conversion. To the best of our knowledge, these are the first Mo,M-mixed oxides reported for the target FAMEs reactions.

The simple and versatile material synthesis methodology can be further explored to prepare multifunctional catalysts, *e.g.*, for integrated acid-oxidation reaction systems. Moreover, these nanomaterials may be interesting for preparing formulated or composite materials for diverse applications.

Author contributions

DMG (formal analysis, investigation, validation, visualization, writing – original draft), PN (supervision, validation, visualization, writing – original draft, resources), XY (formal analysis, investigation), NP (resources, validation, visualization), PAR (conceptualization, methodology, investigation, supervision, validation, resources), AAV (conceptualization, project administration, resources, supervision, validation, visualization, writing – review & editing).

Conflicts of interest

There are no conflicts to declare.

Acknowledgements

This work was developed within the scope of the project CICECO-Aveiro Institute of Materials, UIDB/50011/2020, UIDP/50011/2020 & LA/P/0006/2020, financed by national funds through the FCT/MEC (PIDDAC), and by Project POCI-01-0145-FEDER-030075 (COMPETE 2020 Operational Thematic Program for Competitiveness and Internationalization), co-financed by national funds through the FCT/MCTES and the European Union through the European Regional Development Fund under the Portugal 2020 Partnership Agreement. D. M. G. (grant ref. 2021.04756.BD) acknowledges the FCT for PhD grant (State Budget, European Social Fund (ESF) within the framework of Portugal 2020, namely through the Centro 2020 Regional Operational Program). The authors are very grateful to Doctor M. Rosário Soares (CICECO-Aveiro Institute of Materials) for the discussions and kind assistance with the PXRD studies. C. Erdmann is acknowledged for the TEM measurements. X. Y. thanks the China Scholarship Council (CSC).

References

1 Y. Meng, F. Taddeo, A. F. Aguilera, X. Cai, V. Russo, P. Tolvanen and S. Leveneur, *Catalysts*, 2021, **11**, 765–787.
2 Global Epoxides Market – Industry Trends and Forecast to 2029, **https://www.databridgemarketresearch.com/reports/global-epoxides-market**, (accessed 6 June 2023).
3 P. Bassler, H. G. Göbbel and M. Weidenbach, *Chem. Eng. Trans.*, 2010, **21**, 571–576.
4 Development of New Propylene Oxide Process, **https://www.sumitomo-chem.co.jp/english/rd/report/files/docs/20060100_ely.pdf**, (accessed 17 July 2023).
5 V. Russo, R. Tesser, E. Santacesaria and M. Di Serio, *Ind. Eng. Chem. Res.*, 2013, **52**, 1168–1178.
6 F. Schmidt, M. Bernhard, H. Morell and M. Pascaly, *Chim. Oggi*, 2014, **32**, 31–35.
7 Propylene Oxide Market - Global Forecast to 2026, **https://www.marketsandmarkets.com/Market-Reports/propylene-oxide-market-55659975.html?gclid=Cj0KCQiA1NebBhDDARIsAANiDD3AJLp8tZRYiAyJKcKsAT-YsJKubp9n_IqsaveJNZvRyVTZFPWqsQ4aAhzxEALw_wcB**, (accessed 6 June 2023).
8 V. Smeets, E. M. Gaigneaux and D. P. Debecker, *ChemCatChem*, 2022, **14**, e202101132.
9 A. Corma, S. Iborra and A. Velty, *Chem. Rev.*, 2007, **107**, 2411–2502.
10 G. W. Huber, S. Iborra and A. Corma, *Chem. Rev.*, 2006, **106**, 4044–4098.
11 P. Bajpai, in *Biermann's Handbook of Pulp and Paper*, Elsevier, 3rd edn, 2018, pp. 19–74.
12 A. H. N. Armylisasa, M. F. S. Hazirahb, S. K. Yeonga and A. H. Hazimaha, *Grasas Aceites*, 2017, **68**, e174.
13 Fatty Acid Methyl Ester (FAME) Market Share, Size, Trends, Industry Analysis Report, By Source (Vegetable Oils, Animal Fats, and Used Cooking Oils); By Application; By Region; Segment Forecast, 2022–2030, **https://www.polarismarketresearch.com/industry-analysis/fatty-acid-methyl-ester-fame-market**, (accessed 5 June 2023).
14 W. Yan, Z. Wang, C. Luo, X. Xia, Z. Liu, Y. Zhao, F. Du and X. Jin, *ACS Sustainable Chem. Eng.*, 2022, **10**, 7426–7446.
15 H. Hosney, B. Nadiem, I. Ashour, I. Mustafa and A. El-Shibiny, *J. Appl. Polym. Sci.*, 2018, **135**, 46270–46281.
16 A. Ghosh-Dastidar, S. Kaujalgikar and B. I. Chaudhary, *US Pat.*, 9499681B2, 2016.
17 Y.-Q. Xu and J.-P. Qu, *J. Appl. Polym. Sci.*, 2009, **112**, 3185–3191.
18 R. Belhassen, F. Vilaseca, P. Mutjé and S. Boufi, *Ind. Crops Prod.*, 2014, **53**, 261–267.
19 N. Lv, W. He, Z. Fang, Q. Sun, C. Qiu and K. Guo, *Eur. J. Lipid Sci. Technol.*, 2018, **120**, 1700257–1700264.
20 V. Pantone, C. Annese, C. Fusco, P. Fini, A. Nacci, A. Russo and L. D. Accolti, *Molecules*, 2017, **22**, 333–345.
21 W. F. Hölderich, L. A. Rios, P. P. Weckes, H. Schuster, W. F. Holderich, L. A. Rios and P. P. Weckes, *J. Synth. Lubr.*, 2004, **20**, 289–301.
22 W. He, G. Zhu, Y. Gao, H. Wu, Z. Fang and K. Guo, *Chem. Eng. J.*, 2020, **380**, 122532–122537.
23 C. Kongyai and M. Hunsom, *J. Renewable Sustainable Energy*, 2012, **4**, 053108–053119.
24 K. Wadumesthrige, S. O. Salley and K. Y. S. Ng, *Fuel Process. Technol.*, 2009, **90**, 1292–1299.

25 D. Koziej, M. D. Rossell, B. Ludi, A. Hintennach, P. Novák, J. D. Grunwaldt and M. Niederberger, *Small*, 2011, **7**, 377–387.
26 R. Deshmukh and M. Niederberger, *Chem. – Eur. J.*, 2017, **23**, 8542–8570.
27 J. M. Brégeault, *Dalton Trans.*, 2003, 3289–3302.
28 T. A. Nijhuis, M. Makkee, J. A. Moulijn and B. M. Weckhuysen, *Ind. Eng. Chem. Res.*, 2006, **45**, 3447–3459.
29 G. R. Haas and J. W. Kolis, *Organometallics*, 1998, **17**, 4454–4460.
30 J. Kollar, assignor to Halcon International, Inc., *US Pat.*, 3351635, 1967.
31 K. R. Jain, W. A. Herrmann and F. E. Kühn, *Coord. Chem. Rev.*, 2008, **252**, 556–568.
32 Y. Shen, P. Jiang, P. T. Wai, Q. Gu and W. Zhang, *Catalysts*, 2019, **9**, 31–57.
33 S. Shylesh, M. Jia and W. R. Thiel, *Eur. J. Inorg. Chem.*, 2010, **28**, 4395–4410.
34 I. W. C. E. Arends and R. A. Sheldon, *Appl. Catal., A*, 2001, **212**, 175–187.
35 N. Deligne, D. Bayot, M. Degand and M. Devillers, *J. Solid State Chem.*, 2007, **180**, 2026–2033.
36 C. Tagusagawa, A. Takagaki, K. Takanabe, K. Ebitani, S. Hayashi and K. Domen, *J. Catal.*, 2010, **270**, 206–212.
37 T. Ushikubo, *Catal. Today*, 2000, **57**, 331–338.
38 Niobium and tantalum, **https://www.usgs.gov/publications/niobium-and-tantalum**, (accessed 27 April 2023).
39 Acetophenone, **https://echa.europa.eu/pt/registration-dossier/-/registered-dossier/14683/6/2/1**, (accessed 14 July 2023).
40 K. Skrodczky, M. M. Antunes, X. Han, S. Santangelo, G. Scholz, A. A. Valente, N. Pinna and P. A. Russo, *Commun. Chem.*, 2019, **2**, 1–11.
41 P. Neves, A. C. Gomes, F. A. A. Paz, A. A. Valente, I. S. Gonçalves and M. Pillinger, *Mol. Catal.*, 2017, **432**, 104–114.
42 G. J. Piazza, A. Nuñez and T. A. Foglia, *J. Am. Oil Chem. Soc.*, 2003, **80**, 901–904.
43 L. C. Yang, Q. S. Gao, Y. H. Zhang, Y. Tang and Y. P. Wu, *Electrochem. Commun.*, 2008, **10**, 118–122.
44 L. Wang, K. J. Dong, C. C. Wang, R. P. Zou, Z. Y. Zhou and A. B. Yu, *Powder Technol.*, 2022, **401**, 117217–117226.
45 D. Vollath, *Beilstein J. Nanotechnol.*, 2020, **11**, 854–857.
46 A. Chithambararaj, N. S. Sanjini, A. C. Bose and S. Velmathi, *Catal. Sci. Technol.*, 2013, **3**, 1405–1414.
47 N. Dukstiene, D. Sinkeviciute and A. Guobiene, *Cent. Eur. J. Chem.*, 2012, **10**, 1106–1118.
48 Materials Explorer - MoO2, **https://materialsproject.org/materials/mp-1094123/**, (accessed 19 April 2023).
49 J. A. da Cruz, E. A. Volnistem, R. F. Ferreira, D. B. Freitas, A. J. M. Sales, L. C. Costa and M. P. F. Graça, *Therm. Sci. Eng. Prog.*, 2021, **25**, 101015–101020.
50 H. Ono and K. I. Koyanagi, *Appl. Phys. Lett.*, 2000, **77**, 1431–1433.
51 J. Y. Zhang, Q. Fang and I. W. Boyd, *Appl. Surf. Sci.*, 1999, **138–139**, 320–324.
52 M. R. Mohammadi, D. J. Fray, S. K. Sadrnezhaad and A. Mohammadi, *Mater. Sci. Eng., B*, 2007, **142**, 16–27.
53 F. Z. Tepehan, F. E. Ghodsi, N. Ozer and G. G. Tepehan, *Sol. Energy Mater. Sol. Cells*, 1999, **59**, 265–275.
54 J. Y. Zhang and I. W. Boyd, *Appl. Phys. Lett.*, 2000, **77**, 3574–3576.
55 H. Sun, S. Liu, S. Liu and S. Wang, *Appl. Catal., B*, 2014, **146**, 162–168.
56 R. R. Krishnan, K. G. Gopchandran, V. P. MahadevanPillai, V. Ganesan and V. Sathe, *Appl. Surf. Sci.*, 2009, **255**, 7126–7135.
57 N. Sharma, M. Deepa, P. Varshney and S. A. Agnihotry, *J. Non-Cryst. Solids*, 2002, **306**, 129–137.
58 O. Rezaee, H. Mahmoudi Chenari and F. E. Ghodsi, *J. Sol-Gel Sci. Technol.*, 2016, **80**, 109–118.
59 A. C. Faro, P. Grange and A. C. B. dos Santos, *Phys. Chem. Chem. Phys.*, 2002, **4**, 3997–4007.
60 B. Zhang, S. Xiang, A. I. Frenkel and I. E. Wachs, *ACS Catal.*, 2022, **12**, 3226–3237.
61 K. S. Chung and F. E. Massoth, *J. Catal.*, 1980, **64**, 320–331.
62 L. Wang and W. K. Hall, *J. Catal.*, 1982, **77**, 232–241.
63 E. I. Ross-Medgaarden and I. E. Wachs, *J. Phys. Chem. C*, 2007, **111**, 15089–15099.
64 C. Tiozzo, C. Bisio, F. Carniato, A. Gallo, S. L. Scott, R. Psaro and M. Guidotti, *Phys. Chem. Chem. Phys.*, 2013, **15**, 13354–13362.
65 S. Dworakowska, C. Tiozzo, M. Niemczyk-Wrzeszcz, P. Michorczyk, N. Ravasio, R. Psaro, D. Bogdał and M. Guidotti, *J. Cleaner Prod.*, 2017, **166**, 901–909.
66 E. L. Lee and I. E. Wachs, *J. Phys. Chem. C*, 2007, **111**, 14410–14425.
67 M. Anilkumar and W. F. Hölderich, *J. Catal.*, 2008, **260**, 17–29.
68 F. Hashemzadeh, R. Rahimi and A. Ghaffarinejad, *Ceram. Int.*, 2014, **40**, 9817–9829.
69 M. Baltes, A. Kytökivi, B. M. Weckhuysen, R. A. Schoonheydt, P. Van Der Voort and E. F. Vansant, *J. Phys. Chem. B*, 2001, **105**, 6211–6220.
70 J. H. Praliaud, *J. Less-Common Met.*, 1977, **54**, 387–399.
71 H. Aritani, T. Tanaka, T. Funabiki, S. Yoshida, K. Eda, N. Sotani, M. Kudo and S. Hasegawa, *J. Phys. Chem.*, 1996, **100**, 19495–19501.
72 W. Dong, S. A. Zhou, Y. Ma, D. J. Chi, R. Chen, H. M. Long, T. J. Chun, S. J. Liu, F. P. Qian and K. Zhang, *Rare Met.*, 2023, **42**, 1195–1204.
73 Y. Chang, Y. Zhang, T. Hu, W. Chen, T. Tang, E. Luo and J. Jia, *Molecules*, 2023, **28**, 4739.
74 N. Scotti, N. Ravasio, C. Evangelisti, R. Psaro, M. Penso, P. S. Niphadkar, V. V. Bokade and M. Guidotti, *Catalysts*, 2019, **9**, 334–347.
75 A. Uchagawkar, A. Ramanathan, Y. Hu and Bala Subramaniam, *Catal. Today*, 2020, **343**, 215–225.
76 S. Patnaik, G. Swain and K. M. Parida, *Nanoscale*, 2018, **10**, 5950–5964.
77 J. N. Kondoa, Y. Hiyoshi, R. Osuga, A. Ishikawa, Y.-H. Wang and T. Yokoi, *Materials*, 2018, **262**, 191–198.
78 M. Gancheva, I. Szafraniak-Wiza, R. Iordanova and I. Piroeva, *J. Chem. Technol. Metall.*, 2019, **54**, 1233–1239.

79 X. Yang, N. Wu, Y. Miao and H. Li, *Nanomaterials*, 2018, **8**, 781–797.
80 A. Ogawa and D. P. Curran, *J. Org. Chem.*, 1997, **62**, 450–451.
81 T. R. Amarante, P. Neves, A. A. Valente, F. A. A. Paz, A. N. Fitch, M. Pillinger and I. S. Gonçalves, *Inorg. Chem.*, 2013, **52**, 4618–4628.
82 Y. Kobayashi, S. Inukai, N. Asai, M. Oyamada, S. Ikegawa, Y. Sugiyama, H. Hamamoto, T. Shioiri and M. Matsugi, *Tetrahedron: Asymmetry*, 2014, **25**, 1209–1214.
83 N. Wazir, C. Ding, X. Wang, X. Ye, X. Lingling, T. Lu, L. Wei, B. Zou and R. Liu, *Nanoscale Res. Lett.*, 2020, **15**, 156–164.
84 A. Bento, A. Sanches, E. Medina, C. D. Nunes and P. D. Vaz, *Appl. Catal., A*, 2015, **504**, 399–407.
85 L. F. Veiros, Â. Prazeres, P. J. Costa, C. C. Romão, F. E. Kühn and M. José Calhorda, *Dalton Trans.*, 2006, 1383–1389.
86 P. J. Costa, M. J. Calhorda and F. E. Kühn, *Organometallics*, 2010, **29**, 303–311.
87 M. J. Calhorda and P. J. Costa, *Curr. Org. Chem.*, 2012, **16**, 65–72.
88 P. Sözen-Aktaş, E. Manoury, F. Demirhan and R. Poli, *Eur. J. Inorg. Chem.*, 2013, **15**, 2728–2735.
89 F. E. Kühn, W. M. Xue, A. Al-Ajlouni, A. M. Santos, S. Zang, C. C. Romão, G. Eickerling and E. Herdtweck, *Inorg. Chem.*, 2002, **41**, 4468–4477.
90 J. Pisk and D. Agustin, *Molecules*, 2022, **27**, 6011–6036.
91 P. Jin, D. Wei, Y. Wen, M. Luo, X. Wang and M. Tang, *J. Mol. Struct.*, 2011, **992**, 19–26.
92 A. Comas-Vives, A. Lledós and R. Poli, *Chem. – Eur. J.*, 2010, **16**, 2147–2158.
93 M. Fadhli, I. Khedher and J. M. Fraile, *C. R. Chim.*, 2017, **20**, 827–832.
94 M. H. Furigay, S. Chaudhuri, S. M. Deresh, A. B. Weberg, P. Pandey, P. J. Carroll, G. C. Schatz and E. J. Schelter, *Inorg. Chem.*, 2022, **61**, 23–27.
95 Q. Zhang, X. Li, Q. Ma, Q. Zhang, H. Bai, W. Yi, J. Liu, J. Han and G. Xi, *Nat. Commun.*, 2017, **8**, 14903–14911.
96 W. Zhang, L. Xing, J. Chen, H. Zhou, S. Liang, W. Huang and W. Li, *J. Alloys Compd.*, 2020, **822**, 153530–153536.
97 Y. Sun, X. Hu, W. Luo and Y. Huang, *J. Mater. Chem.*, 2012, **22**, 425–431.
98 P. A. Abramov and M. N. Sokolov, *Molecules*, 2023, **28**, 4912–4923.
99 C. Tiozzo, C. Bisio, F. Carniato, L. Marchese, A. Gallo, N. Ravasio, R. Psaro and M. Guidotti, *Eur. J. Lipid Sci. Technol.*, 2013, **115**, 86–93.
100 Y. B. Huang, M. Y. Yao, P. P. Xin, M. C. Zhou, T. Yang and H. Pan, *RSC Adv.*, 2015, **5**, 74783–74789.
101 G. B. Bantchev, K. M. Doll, G. Biresaw and K. E. Vermillion, *J. Am. Oil Chem. Soc.*, 2014, **91**, 2117–2123.
102 K. Herman and J. Foodtechn, *Fat Sci. Technol.*, 1995, **97**, 269–273.
103 T. Kitano, S. Okazaki, T. Shishido, K. Teramura and T. Tanaka, *J. Mol. Catal. A: Chem.*, 2013, **371**, 21–28.
104 D. M. Gomes, P. Neves, M. M. Antunes, A. J. S. Fernandes, M. Pillinger and A. A. Valente, *Catalysts*, 2022, **12**, 1513.
105 X. Gao, Y. Zhang, Y. Hong, B. Luo, X. Yan and G. Wu, *Microporous Mesoporous Mater.*, 2022, **333**, 111731–111740.
106 E. Ucciani, A. Debal and G. Rafaralahitsimba, *Fat Sci. Technol.*, 1993, **95**, 236–239.
107 M. Guidotti, N. Ravasio, R. Psaro, E. Gianotti, L. Marchese and S. Coluccia, *Green Chem.*, 2003, **5**, 421–424.
108 M. Guidotti, I. Batonneau-Gener, E. Gianotti, L. Marchese, S. Mignard, R. Psaro, M. Sgobba and N. Ravasio, *Microporous Mesoporous Mater.*, 2008, **111**, 39–47.